OPEN

Citation: Cell Death and Disease (2013) 4, e797; doi:10.1038/cddis.2013.332

www.nature.com/cddis

Loss of Pde6 reduces cell body Ca^{2+} transients within photoreceptors

EY Ma[1], A Lewis[1], P Barabas[2], G Stearns[1], S Suzuki[3], D Krizaj[2] and SE Brockerhoff*[,1]

Modulation of Ca^{2+} within cells is tightly regulated through complex and dynamic interactions between the plasma membrane and internal compartments. In this study, we exploit *in vivo* imaging strategies based on genetically encoded Ca^{2+} indicators to define changes in perikaryal Ca^{2+} concentration of intact photoreceptors. We developed double-transgenic zebrafish larvae expressing GCaMP3 in all cones and tdTomato in long-wavelength cones to test the hypothesis that photoreceptor degeneration induced by mutations in the phosphodiesterase-6 (Pde6) gene is driven by excessive $[Ca^{2+}]_i$ levels within the cell body. Arguing against Ca^{2+} overload in Pde6 mutant photoreceptors, simultaneous analysis of cone photoreceptor morphology and Ca^{2+} fluxes revealed that degeneration of *pde6c*^{w59} mutant cones, which lack the cone-specific cGMP phosphodiesterase, is not associated with sustained increases in perikaryal $[Ca^{2+}]_i$. Analysis of $[Ca^{2+}]_i$ in dissociated *Pde6β*^{rd1}mouse rods shows conservation of this finding across vertebrates. *In vivo*, transient and Pde6-independent Ca^{2+} elevations ('flashes') were detected throughout the inner segment and the synapse. As the mutant cells proceeded to degenerate, these Ca^{2+} fluxes diminished. This study thus provides insight into Ca^{2+} dynamics in a common form of inherited blindness and uncovers a dramatic, light-independent modulation of $[Ca^{2+}]_i$ that occurs in normal cones.

Cell Death and Disease (2013) **4,** e797; doi:10.1038/cddis.2013.332; published online 12 September 2013
Subject Category: Neuroscience

Photoreceptor degeneration is a devastating disease that affects millions of people worldwide. Mutations that alter cyclic guanosine-mono-phosphate (cGMP) levels are a common cause of photoreceptor degeneration; mutations in guanylate cyclase, guanylate cyclase-activating proteins, phosphodiesterase-6 (Pde6) and the Pde6 chaperone, aryl hydrocarbon receptor interacting protein-like 1, all cause loss of rods and/or cones (Retinal Information Network, https://sph.uth.edu/retnet/home.htm). The precise mechanism of cGMP-mediated cell death is poorly defined, and thus animal models are particularly relevant to study as a tool to help cure and treat this disease.

The most studied animal model for photoreceptor degeneration due to elevated cGMP is the *rd1* mouse, identified more than 90 years ago.[1,2] *rd1* mice have a mutation in the beta subunit of rod cGMP Pde6, a key mediator of the light response.[3,4] Normally, light activates a molecular cascade that causes Pde6 to hydrolyze cGMP, resulting in closure of cation channels within the photoreceptor outer segment (OS). In the absence of Pde6 beta in *rd1* mice, cGMP levels remain elevated and rod photoreceptors start to degenerate after their differentiation and before eye opening.[3] Cone photoreceptors lacking Pde6c also have elevated cGMP in their OSs.[5] Elevated cGMP is proposed to result in sustained increases in OS Ca^{2+}, triggering death. Consistently, elevated OS Ca^{2+} was measured in hypomorphic Pde6 mutant rods[6] and rod viability was recently shown to improve in *Cngb1*$^{(-/-)}$ × *Pde6β*^{rd1}double-mutant mice.[7] However, the degeneration processes take place within the perikaryon, not the OS. Thus, a key challenge has been to determine the signaling pathways through which elevated cGMP and Ca^{2+} within OSs of Pde6 mutant cells affect photoreceptor cell biology downstream from the OS.

Although events associated with non-apoptotic cell death pathways such as poly-ADP-ribose-polymerase and calpain activation occur in rods dying due to elevated cGMP,[8,9] the molecular cascade activated in degenerating Pde6 mutant photoreceptors is unknown. Specifically, involvement of Ca^{2+} in the *rd1* pathology is a major unsolved question.[10] It is often assumed that elevated Ca^{2+} within OSs triggers cell death by activating Ca^{2+}-dependent mechanisms within the cell body.[11] However, cGMP and Ca^{2+} diffusion from the OS to the inner segment are likely to be limited by anatomical constraints (the ciliary bottleneck), buffering and the ellipsoid mitochondrial barrier.

To ascertain the role of Ca^{2+} in photoreceptor degeneration caused by loss of Pde6, it is necessary to measure this ion within the inner segment. We therefore generated here a double-transgenic zebrafish, transgenic (*Tg*; *Trß2:tdTomato; TαCP:GCaMP3),* in which the Ca^{2+} indicator GCaMP3 is selectively expressed in the photoreceptor cell body, not the OS. We recorded Ca^{2+} dynamics within intact cones from

[1]Department of Biochemistry, University of Washington, Seattle, WA, USA; [2]Department of Ophthalmology & Visual Sciences, Moran Eye Center, University of Utah School of Medicine, Salt Lake City, UT, USA and [3]Department of Biological Structure, University of Washington, Seattle, WA, USA
*Corresponding author: SE Brockerhoff, Department of Biochemistry, UW, Seattle, WA 98195, USA. Tel: 206-616-9464; Fax: 206 685 1792; E-mail: sbrocker@uw.edu
Keywords: calcium; zebrafish; neurodegenerative disease; photoreceptors; phosphodiesterases
Abbreviations: cGMP, cyclic guanosine-mono-phosphate; Pde6, phosphodiesterase-6; OS, outer segment; d.p.f., days post fertilization; WT, wild type; RP, retinitis pigmentosa; PTU, 1-phenyl 2-thiourea; ERG, electroretinogram; *TαCP*, cone α-transducin promoter; $[Ca^{2+}]_i$, intracellular calcium; ROI, region of interest; Tg, transgenic; *Trβ2*, thyroid hormone receptor β2; GFP, green flourescent protein; mCFP, membrane cyan fluorescent protein
Received 21.6.13; revised 21.7.13; accepted 29.7.13; Edited by A Stephanou

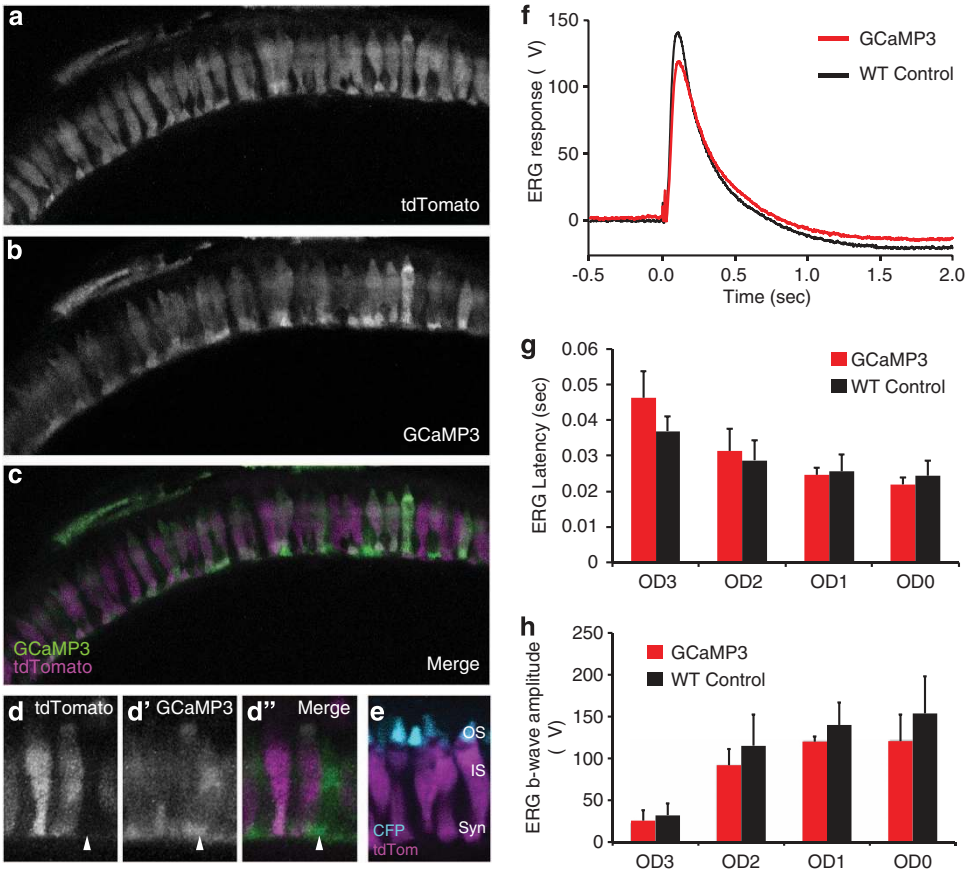

Figure 1 GCaMP3 is expressed in all cone photoreceptors and does not interfere with light responses. (**a**–**c**) Retinal slice projections from a representative 5 d.p.f. *Tg(Trß2:tdTomato;TαCP:GCaMP3)* double-transgenic *pde6c*^{w59} mutant zebrafish larvae displaying intact photoreceptors prior to their degeneration. The tdTomato (**a**) is expressed only in long-wavelength cones, whereas the GCaMP3 (**b**) is expressed in all cone photoreceptors. Panel **c** shows both tdTomato (magenta) and GCaMP3 (green) channels merged. (**d**) Magnified view of cone photoreceptors in the *Tg(Trß2:tdTomato;TαCP:GCaMP3)* double transgenic. Arrow indicates a cell expressing GCaMP3 (green) but not tdTomato (magenta). Less expression of both GCaMP3 and tdTomato is observed in the cone outer segments (OS), whose location within the photoreceptor layer is clearly defined by the *TαCP:membrane CFP* (membrane cyan fluorescent protein (*mCFP*); cyan) transgene (**e**) Retinal section from a *Tg(Trß2:tdTomato; TαCP:mCFP)* double-transgenic fish expressing tdTomato in long-wavelength cones (magenta) and membrane CFP (cyan) in all cones. The outer segments (OS), inner segments (IS), and synapses (syn) are as indicated. (**f**–**h**) ERG waveforms (**f**), b-wave latencies (**g**), and b-wave amplitudes (**h**) for 5 d.p.f. WT non-transgenic *versus Tg(TαCP:GCaMP3)* larvae show no significant differences in their light responses over three orders of magnitude. $n = 3$ fish per condition; bars = S.D.

wild type (WT) and mutant (*pde6c*^{w59}) retinas using multi-photon time-lapse imaging. *pde6c*^{w59} cones degenerate starting immediately after their differentiation at 4 days post fertilization (d.p.f.), and are mostly lost by 7 d.p.f.[12,13] This mutation is thus analogous to the well-characterized rod *Pde6β*^{rd1}mutation.[3,4] To confirm our results in the mammalian model, we extended our approach to record intracellular Ca^{2+} ($[Ca^{2+}]_i$) levels in *rd1* mouse rods.

By combining the power of zebrafish genetics with live, noninvasive imaging, we were able to follow Ca^{2+} signaling within degenerating vertebrate cones in real-time. Surprisingly, we did not detect sustained $[Ca^{2+}]_i$ increases in *pde6c*^{w59} mutant cones nor were abnormalities in baseline $[Ca^{2+}]_i$ observed in degenerating *rd1* mouse rods. Ca^{2+} signals in non-mutant and *pde6c*^{w59} mutant zebrafish cones include recurring transient $[Ca^{2+}]_i$ increases ('flashes'), consistent with complex regulation of the Ca^{2+} homeostatic apparatus within the photoreceptor regions downstream from the OS. Our results thus challenge the prevailing view that *rd1* degeneration is driven by global Ca^{2+} elevations that overload the endogenous Ca^{2+} buffering and clearance mechanisms within the cell body, and thus have implications for the development of neuroprotection strategies in retinitis pigmentosa (RP) models of retinal degeneration.

Results

We constructed a transgenic line expressing GCaMP3 specifically in zebrafish cones using the cone transducin promoter (*TαCP)* that we previously isolated.[14] GCaMP3 is a fluorescent Ca^{2+} indicator consisting of circularly permuted green fluorescent protein (GFP), calmodulin, and the Ca^{2+}-calmodulin target peptide M13.[15] GCaMP3 has increased fold fluorescence change (increased Fmax/Fmin) and higher Ca^{2+} affinity (660 ± 19 nm) than many other genetically encoded indicators.[15] It is widely used as an indicator of *in vivo* changes in intracellular Ca^{2+}.[16–18] In zebrafish cones, GCaMP3 localizes throughout the cone cytoplasm, but is less abundant in the OS (Figures 1b–e). We then generated double transgenics by crossing the *Tg(TαCP:GCaMP3)* strain

with a transgenic fish line expressing the fluorescent protein tdTomato selectively in long-wavelength cone photoreceptors using the thyroid hormone receptor $\beta 2$ promoter, *Tg(Trβ2:tdTomato)* (Williams *et al.*[19] and Figures 1a and c–e). The tdTomato fluorescence in long-wavelength cones has several uses. Uniform cytoplasmic distribution of tdTomato facilitates visualization of the overall cell shape so that morphological changes during cell death can be analyzed. Further, its expression in a subset of discretely spaced cones defines these cells for visual analysis, and serves as a photobleaching control. Double-transgenic fish (*Tg(Trβ2:tdTomato; TαCP:GCaMP3)*) were used for live imaging experiments, where we directed our observation of Ca^{2+} dynamics to the cone photoreceptor cell body and synaptic terminal.

ERG analysis of transgenic GCaMP3 cones. A potential problem when expressing fluorescent indicators of intracellular Ca^{2+} is the disruption of Ca^{2+} homeostasis due to abnormal buffering. To ensure that GCaMP3 expressed in cones does not alter normal fluxes in Ca^{2+}, we measured electroretinogram (ERG) responses from our transgenic line and compared these with WT ERG responses. ERGs were recorded from excised eyes as previously described.[20] If introduction of excess buffer affected the photoreceptor $[Ca^{2+}]_i$, the delay and/or reduction in synaptic signaling would be detected as a diminished and/or delayed ERG b-wave. We found that the ERG waveforms appeared similar, and no significant differences in b-wave amplitude or latency between transgenic and non-transgenic WT cones were observed (Figures 1f–h). These results indicate that the GCaMP3 transgene does not significantly alter the visual responses of photoreceptors.

Ca^{2+} dynamics in dying zebrafish cones. Our previous characterization of the *pde6c*^{w59} mutant used multiphoton imaging to analyze morphological changes associated with cone photoreceptor cell death that occur *in vivo*.[12] Mutant cells differentiate normally and appear morphologically normal, with small OSs and extended synaptic processes, until $\sim$4 d.p.f. The mutant cells then proceed through a series of morphological changes prior to their clearance from the retina. Typically, the synapse is first retracted, followed by the contraction of the OS and the rounding of the cell body. These morphological changes occur asynchronously across the retina over 2–3 days; by 7 d.p.f. the vast majority of cones are gone in the mutant retina. In an individual cell, morphological changes occur over $\sim$8 h (Lewis *et al.*[12] and Figure 2b). Based on recent studies in the *rd1* mouse, morphological changes associated with cell death in *pde6c*^{w59} cones are likely late in the cell death cascade.[21]

To examine Ca^{2+} dynamics during cell death, we monitored both changes in GCaMP3 fluorescence and in cell shape at 20 min intervals in time-lapse experiments that extended up to 9 h. We then quantified changes in GCaMP3 fluorescence in dying cells that initially appeared morphologically normal at the beginning of the time-lapse, but had completely rounded up by the end of the experiment. As a proof of principle for this study, we initially caused death of non-mutant cells by intense infrared laser illumination via multiphoton time-lapse imaging. This method led to profound increases in GCaMP3 fluorescence that saturated our detectors (Figures 2a and c). During the dying process of these laser-damaged cells, dramatic localized increases in GCaMP3 fluorescence typically around the nucleus were observed. These initial GCaMP3 changes were either transient or sustained, but were consistently followed by dramatic persistent increases that extended throughout the entire cell body as the photoreceptor rounded up (Figure 2a).

We used optimized multiphoton imaging conditions that do not damage homozygous *pde6c*^{w59} cones[12] to monitor GCaMP3 fluorescence changes in mutant cells that degenerate during the 9 h time-lapse. In contrast to the dramatic changes observed with laser-induced death, we did not detect pronounced intracellular increases in GCaMP3 fluorescence in the *pde6c*^{w59} mutant dying photoreceptors (Figure 2b). We quantified intracellular fluorescent changes in 19 individual cells from four different fish, and none of these cells showed sustained increases in GCaMP3 fluorescence over time (Figure 2c). Even though the average change in cell body fluorescence centered at zero for these 19 cells, the specific changes in individual cells were unique. Some cells showed very little change, some decreased in overall fluorescence, whereas others showed recurring small transient increases in GCaMP3 fluorescence (Figure 2d and Figure 4).

Ca^{2+} dynamics in dying mouse rods. To determine whether our finding represented a general feature of RP-like photoreceptor degeneration across vertebrates, we extended our measurements to intracellular Ca^{2+} in rod photoreceptors from *rd1* mice, arguably the most widely used model of Pde6 dysfunction.[7–11] Intracellular Ca^{2+} was assessed in acutely isolated *rd1* rods and age-matched WT cells at the start of degeneration (postnatal day 8–10), and at the peak of degeneration after eye opening (postnatal day 14–21). The cells were identified by shape, size and/or expression of GFP (Figure 3b).[22] Figure 3a illustrates averaged data from 19 simultaneously recorded *rd1* rods loaded with the Ca^{2+} indicator Fura-2. The calibration protocol shows baseline ratio values for dissociated light-adapted rods, followed by decreased ratio in Ca^{2+} free saline (possibly mediated by the closure of store-operated channels)[22] and then ionomycin-induced Ca^{2+} release from internal stores. The inset displays calibrated $[Ca^{2+}]_i$ with stable baseline levels maintained at $\sim$50 nM. $[Ca^{2+}]_i$ levels in developing rods were comparable to concentrations measured in adult WT cells.[22] Consistent with *in vivo* measurements in intact teleost cones, baseline $[Ca^{2+}]_i$ in dissociated *rd1* rod somata was not significantly elevated before or during cGMP-driven rod degeneration even at ages P14–21 during massive rod loss (Figure 3c).

Ca^{2+} oscillations in pde6c^{w59} zebrafish cone photoreceptors. We next analyzed the Ca^{2+} oscillations that we detected in zebrafish cones to determine how these related to the cell death process. We found that 27% of *pde6c*^{w59} mutant cones ($n=84$) exhibited oscillations in GCaMP3 fluorescence during our 9-hr time-lapse experiments. The intensity of oscillations varied from cell to cell and even within cells, thus we used a change in intensity of $\sim$18% as a lower limit for our definition of an increase.

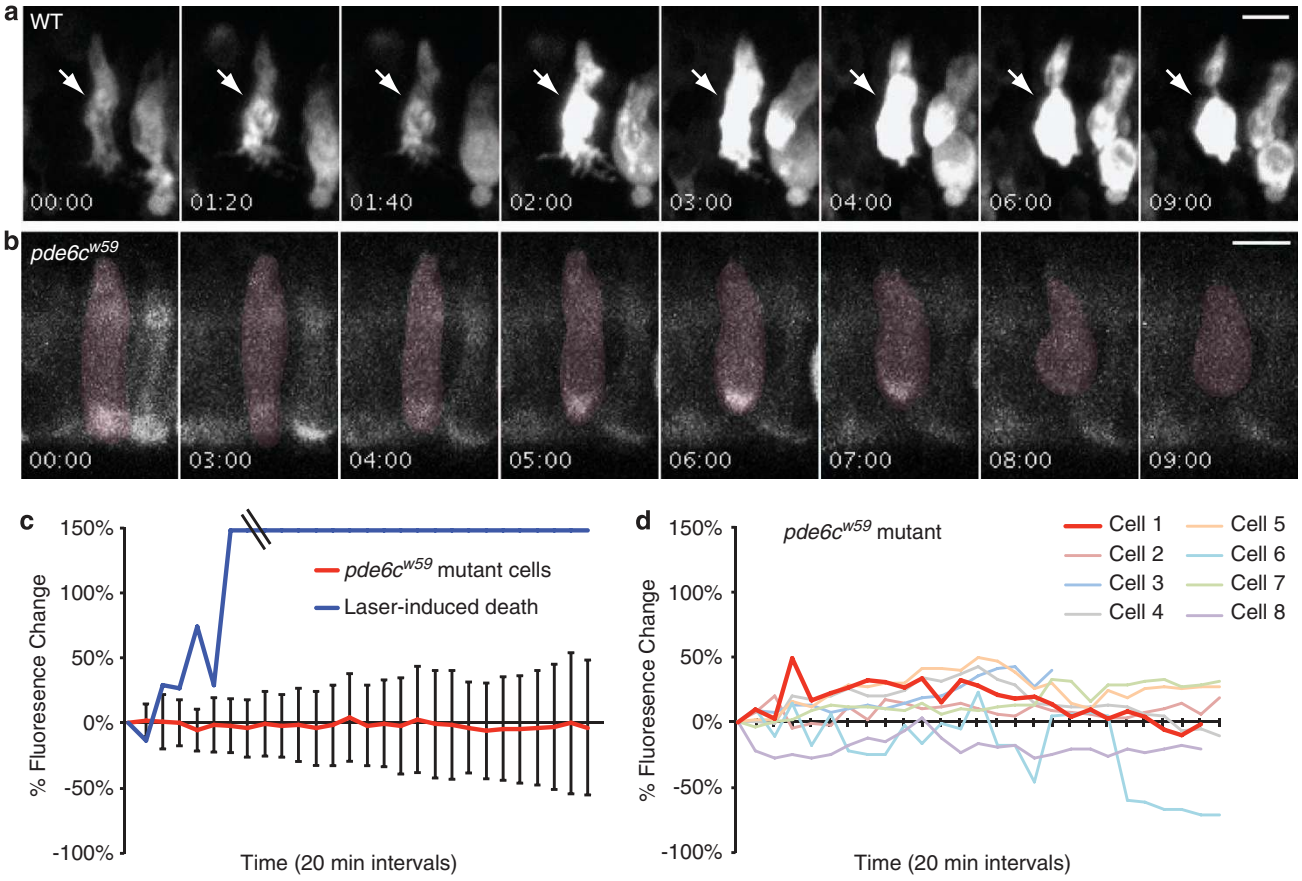

Figure 2 Modest and variable changes in Ca^{2+} occur during the death of *pde6c*^{w59} cones. Photoreceptors from 5—6 d.p.f. larvae expressing *TαCP:GCaMP3* were imaged every 20 min for 9 h. (**a**, **b**) Montages of representative cells at select time points show GCaMP3 fluoresence and morphology changes in dying photoreceptors for both *pde6c*^{w59} heterozygous (**a**) and *pde6c*^{w59} homozygous (**b**) photoreceptors. Time = (h:min). (**c**) Graph showing mean percentage of fluorescence change of GCaMP3 from 19 *pde6c*^{w59} mutant cells undergoing cGMP-mediated death (bars = S.D.) and the single representative laser-induced dying cell shown in **a**. Laser power and time of exposure was increased to stimulate laser-induced death of non-mutant cones. In addition, these cells were more sensitive than the homozygous *pde6c*^{w59} cones to prolonged laser exposure. For homozygous *pde6c*^{w59}mutants, laser conditions were optimized to not cause morphological defects during the extended time-lapses. (**d**) Graph showing variations in percentage of GCaMP3 fluorescence changes in eight individual cones from a single *pde6c*^{w59} mutant fish. The red line (cell 1) indicates the percentage of change in GCaMP3 fluorescence of the representative dying *pde6c*^{w59} mutant cone shown in **b**

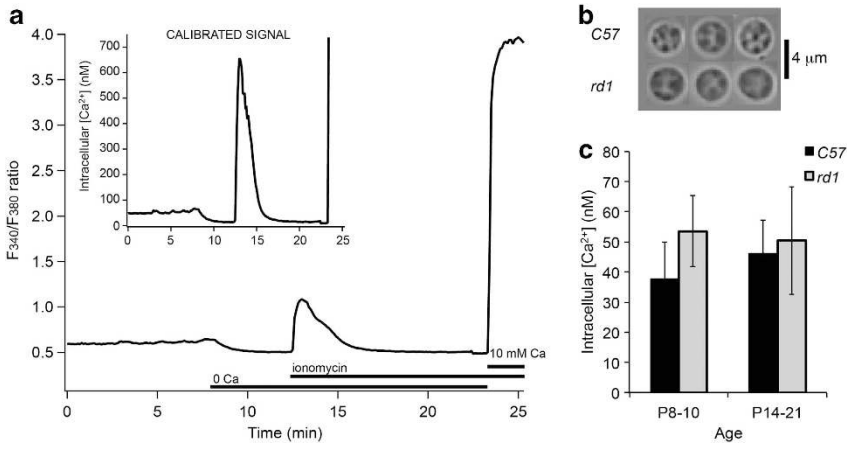

Figure 3 Ca^{2+} measurements in dying mouse rods. (**a**) Average ($n = 19$) fluorescence ratio and calibrated signal during baseline calcium measurements from acutely isolated *Pde6β*^{rd1} (*rd1*) mouse rod perikarya at P10. Ionomycin was used to clamp intracellular calcium levels to external zero calcium (containing 1 mM EGTA to obtain Rmin) or 10 mM calcium level (to obtain Rmax), allowing for a cell-by-cell calibration of the fluorescent signal. (**b**) Typical morphology of *C57Bl6J* (*C57*) or *rd1* mouse rod photoreceptors. (**c**) No significant differences in absolute baseline Ca^{2+} concentration of acutely isolated *C57Bl6J* (*C57*) or *Pde6β*^{rd1} (*rd1*) mouse rod perikarya at ages between 8 and 10 days and 14 and 21 days were observed. Shown are group averages ± S.E.M. p8–10: 37.7 ± 12.2 (*C57*), 53.5 ± 11.8 (*rd1*); p14–21: 46.2 ± 11.0 (*C57*), 50.4 ± 17.8 (*rd1*)

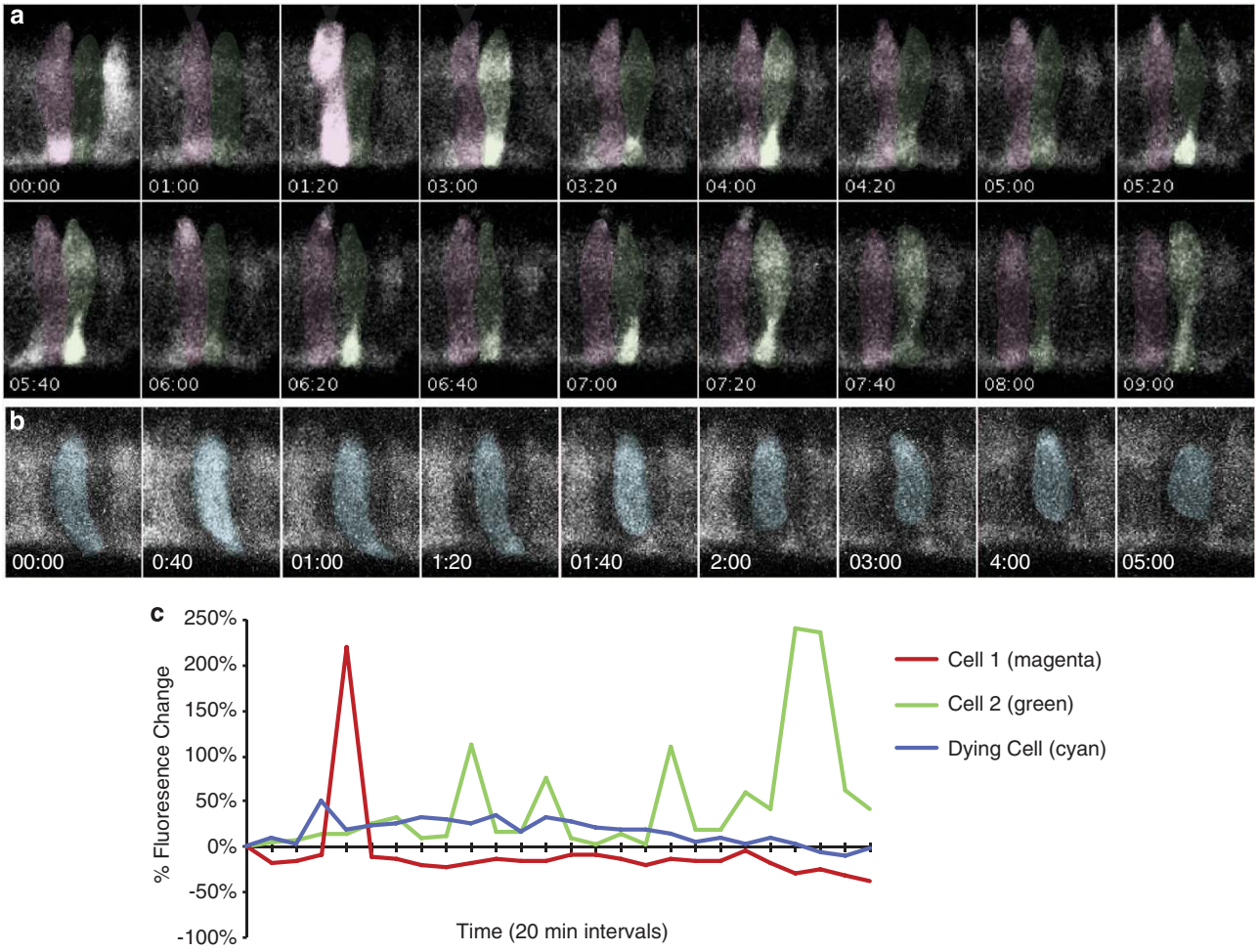

Figure 4 Ca^{2+} oscillations occur in morphologically normal and dying *pde6c*^{w59} cones. Photoreceptors from homozygous *pde6c*^{w59} double-transgenic animals *Tg(Trß2:tdTomato;TαCP:GCaMP3)* were imaged every 20 min. Only the GCaMP3 channel is shown. (**a**, **b**) Montages of representative morphologically normal (**a**) and degenerating (**b**) *pde6c*^{w59} cones show transient increases in GCaMP3 fluorescence. Time = (h:min). (**c**) Graph of percentage change in GCaMP3 fluorescence intensity for outlined cells shown in **a** and **b**. Oscillations in GCaMP3 fluorescence occur at random intervals throughout the time-lapse in morphologically normal cones, whereas transient increases in dying cells usually occur near the beginning of the time-lapses (**c** and Figure 2d)

GCaMP3 increases occurred both simultaneously throughout the cell body and synapse, or were often localized only to the synaptic region (Figure 4a). Both morphologically normal cells (Figures 4a and c) and those undergoing morphological changes (Figures 4b and c) exhibited Ca^{2+} oscillations. For the dying cells that eventually rounded up, the most significant increase(s) in $[Ca^{2+}]_i$ occurred at the beginning of the time-lapse before any major cell shape changes were observed (Figures 4b and c).

To analyze the temporal and spatial characteristics of these recurring transient GCaMP3 increases in greater detail, we conducted shorter time-lapse experiments (ranging from 15–30 min) and acquired images every 5 s. Image acquisition every 5 s allowed sampling of a single retinal plane containing ~30–50 cells. As the overall experiment was short, we focused our analysis on the *pde6c*^{w59} mutant cone cells that appeared morphologically normal throughout the experiment. A representative experiment and subsequent data analysis is shown in Figure 5. Using this rapid imaging paradigm, rapid recurring Ca^{2+} increases ('flashes') were observed in many cells within this imaged population (see Supplemental Movie). For example, in the representative cell shown in Figure 5a, a bright increase is observed in the synapse at 0905 hours, but is not seen in the time point before (0900 hours) nor after (0910 hours). Another synaptic increase is seen in the same cell at 0915 hours, is gone at 0920 hours, and reoccurs at 0925 hours. This analysis indicates that these particular flashes lasted for 5 s or less. To optimize our analysis of multiple *pde6c*^{w59}photoreceptor cells in a single retinal population, we straightened our retinal images (Figure 5b) and generated kymographs (Figure 5c). Two kymographs were generated for each time-lapse; one for the synapse and one for the cell body. These kymographs are overlaid in two different colors in Figure 5c. Green shows GCaMP3 fluorescence increases localized to the synapse regions and magenta shows Ca^{2+} changes throughout the cell body (Figure 5c).

Using our kymographs, we graphed the GCaMP3 signal intensity over time for each photoreceptor and established general categories describing the types of flashes we

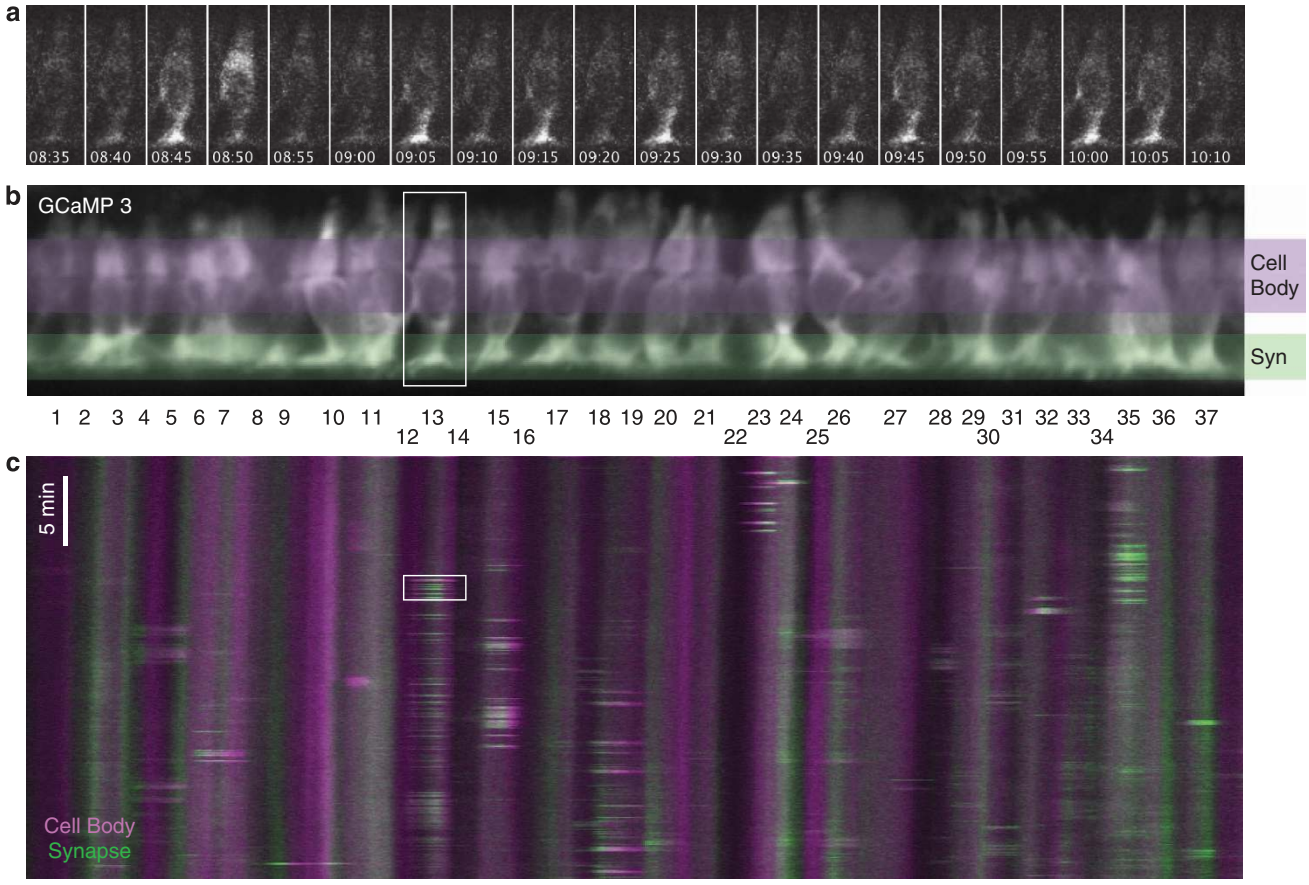

Figure 5 Recurrent Ca^{2+} flashes are variable, rapid, asynchronous, and prevalent. Photoreceptors from homozygous double-transgenic *Tg(Trß2:tdTomato;TαCP:GCaMP3) pde6c*^{w59} fish were rapidly imaged every 5 s for 15–30 min. Only the GCaMP3 channel is shown. (**a**) Montage of a representative cell (cell 13; see **b** and **c**) at select time points show rapid transient increases in GCaMP3 fluorescence occurring in both the cell body and synapse. Time = (min:s). (**b**) Representative image (time) projection from a straightened *Tg(Trß2:tdTomato;TαCP:GCaMP3) pde6c*^{w59} retina shows GCaMP3 fluorescence in all cones. The shaded areas represent the areas used to generate the kymograph (**c**) for the cell body (magenta) and for the synapse (syn; green). All identifiable cells are numbered below and correspond to a column on the kymograph in **c**. (**c**) Representative kymograph of GCaMP3 signal across all the time points for both the cell body (magenta) and synapse (green). The boxed areas on both the kymograph (**c**) and the straightened retina (**b**) represent the cell (cell 13) and time period shown in the montage in **a**

detected. Cells that flashed fewer than 10 times over 30 min were labeled as 'infrequent,' whereas those flashing more than 10 times were categorized as 'frequent'. Cells that flashed infrequently were also subdivided based upon the duration of the flashes. Cells whose infrequent flashes lasted for only 1–3 time points were deemed as 'infrequent rapid', whereas 'infrequent mixed' cells exhibit flashes that were sustained over several time points (Figures 6a and b). Cells with frequent flashes exhibited transient GCaMP3 increases of mixed duration (Figure 6c), but a few cells showed recurring transient increases that lasted over an extended period of time (categorized as 'frequent extended'), often with varying intensities within the elevated GCaMP3 signal (Figure 6d). A few cells also showed a change in fluorescence, either increasing or decreasing, that persisted throughout the time-lapse. This small number of cells was categorized in the 'other' category. From our analysis of 447 cells from 11 *pde6c*^{w59}fish, we determined that 46% of cells flash during the 15–30 min time-lapse experiments, and that there were roughly equal number of cells that flash infrequently (both rapid and mixed) and those that flash frequently. Consistent with our longer time-lapse experiments, extended increases in fluorescence were detected in only a few cells (Figure 6e).

Ca^{2+} dynamics in non-mutant cone photoreceptors. As Ca^{2+} flashes within photoreceptors have not been reported previously, we speculated that elevated cGMP and consequent metabolic changes in *pde6c*^{w59}cones disrupt Ca^{2+} homeostasis, causing transient increases in $[Ca^{2+}]_i$. To examine this possibility, we analyzed flashes in photoreceptors from both WT and *pde6c*^{w59} heterozygous fish, siblings of the *pde6c*^{w59} mutants previously analyzed, and imaged these photoreceptors *in vivo* at 5 s intervals for 15–30 min. We noted that the light-sensitive cones from WT and *pde6c*^{w59} heterozygous fish were more sensitive to laser exposure than the light-insensitive homozygous *pde6c*^{w59} photoreceptors. Slight laser-induced morphological abnormalities were detected in some photoreceptors during imaging, and data were not analyzed from these cells.

To our surprise, kymograph analysis of cone photoreceptors from WT and *pde6c*^{w59} heterozygous fish ($n = 263$ cells; 6 fish) revealed the same categories of flashes as observed in

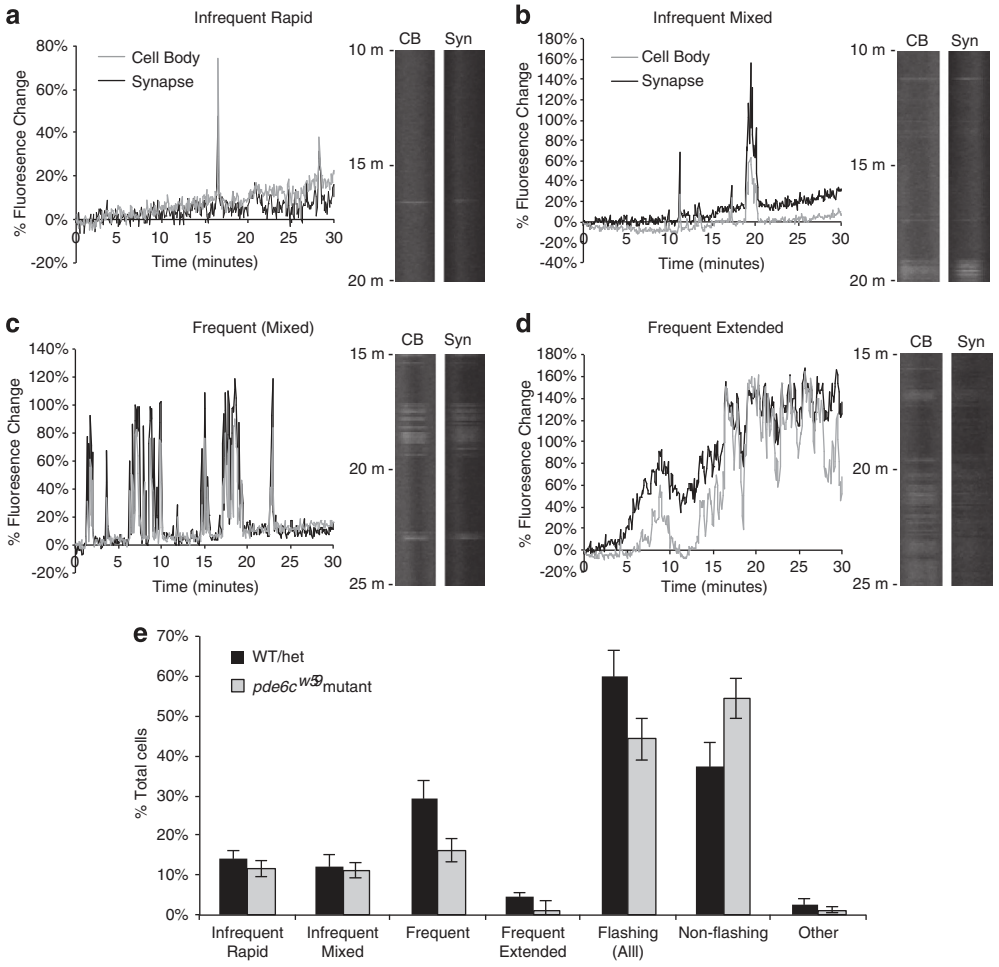

Figure 6 Characterization of heterogeneous Ca^{2+} flashes show fewer *pde6c*^{w59} mutant cones with frequent flash patterns. Individual cones from kymographs of the rapid 5 s time-lapse imaging experiments were analyzed and categorized according to their pattern of GCaMP3 flashes. (**a**–**d**) Representative graphs and kymograph segments of GCaMP3 flash patterns in both the cell body (CB) and synapse (syn) of cones. Flashing cells were categorized into four main categories: 'infrequent rapid' (**a**), 'infrequent mixed' (**b**), 'frequent' (**c**), and 'frequent extended' (**d**). See text for more details regarding flash categorization. (**e**) Graph showing the percentage of various categories of flashing cells in both *pde6c*^{w59} mutant and non-mutant (WT/het) cones. The 'other' category consists of a small number of non-flashing cells that showed persistent increasing or decreasing GCaMP3 fluorescence throughout the duration of the time-lapse (**e**). Overall, fewer cells exhibiting Ca^{2+} flashes were observed in *pde6c*^{w59} mutants than in WT/het larval retinas ('Flashing (All)'), largely due to a reduction in the 'frequent' category. No significant difference in mutant and non-mutant cones was observed in the other categories. For *pde6c*^{w59}mutants: $n = 447$ cells; 11 fish. For WT/het: $n = 263$ cells; six fish. Bars = S.E.M.

the *pde6c*^{w59}mutant photoreceptors. Further, our results indicated that altered metabolism due to elevated cGMP did not increase the number of cells flashing or the flash frequency of individual cells, but rather decreased these; 44% of mutant cells flashed *versus* 60% of non-mutant cones ($P = 0.09$), and this reduction in flashing *pde6c*^{w59} mutant cones was primarily cells categorized as 'frequent' (16% mutant *versus* 29% non-mutant, $P = 0.03$, Figure 6e).

Taken together, these data show that dynamic modulation of $[Ca^{2+}]_i$ occurs in WT cone photoreceptors and that this modulation is mostly retained in light-insensitive *pde6c*^{w59} mutant cones prior to their degeneration, although fewer frequently flashing cells were observed. However, at late stages of death when mutant cells degenerate, Ca^{2+} transients are substantially reduced or cease and catastrophic Ca^{2+} release into the cytoplasm does not occur.

Discussion

In this study, we report an *in vivo* analysis of Ca^{2+} dynamics in cone photoreceptors within a host animal. We exploit a double-transgenic zebrafish that enables simultaneous analysis of cytoplasmic changes in Ca^{2+} and of overall changes in cell morphology, and extend our analysis of Ca^{2+} regulation in *pde6c*^{w59} cones to the commonly studied *rd1* mouse model. We discovered that (1) *pde6c*^{w59} mutant cone photoreceptors and *rd1* rods do not exhibit sustained intracellular Ca^{2+} increases during degeneration; (2) transient Ca^{2+} increases are prevalent in *pde6c*^{w59} mutant and non-mutant cone photoreceptors; (3) these Ca^{2+} flashes occur throughout the cell body and synapse, or are only localized to the synapse; (4) Ca^{2+} transients vary in frequency and duration; and (5) fewer cells in the *pde6c*^{w59} mutant retinas show a pattern of frequent recurring Ca^{2+} flashes compared with non-mutant retinas. Our findings shed light on the mechanism of cell death occurring in *pde6c*^{w59}

mutant cones and *rd1* rods, and highlight a potentially functionally important measure of normal cone photoreceptor physiology.

Pde6 is a key mediator of the well-established vertebrate phototransduction cascade. Activated by GTP-bound α-transducin, it hydrolyzes cGMP, resulting in closure of cation channels in the OS plasma membrane. Loss of Pde6 activity increases OS Ca^{2+} levels[6] possibly causing cell death, a conjecture supported by the observation that reducing Ca^{2+} influx by knocking out cGMP-gated cation channels (*Cngb1*$^{(-/-)}\times$ *Pde6β*^{rd1}) improves viability of *rd1* rods.[7] However, to understand the physiological coupling between $[Ca^{2+}]_i$ and the degeneration process, it is necessary to ascertain Ca^{2+} dynamics within the inner segment. We therefore developed a novel zebrafish transgenic line, *Tg(Trß2:tdTomato;TαCP:GCaMP3),* and compared Ca^{2+} signals obtained in degenerating *pde6c*^{w59}cones with $[Ca^{2+}]_i$ levels within the *Pde6β*^{rd1} rods. To avoid interference from signals emanating from over-activation of Ca^{2+} fluxes through cGMP channels,[7] *pde6c*^{w59}mutants were designed to express the genetically encoded Ca^{2+} indicator GCaMP3 within cell compartments downstream from the OS.

One possible mechanism for *pde6c*^{w59}and *rd1* photoreceptor degeneration was mitochondrial Ca^{2+} overload and a consequent increase in cytosolic $[Ca^{2+}]_i$ within the perikaryon.[23] Using live imaging, we detected modest changes in intracellular Ca^{2+} that varied between individual dying cells; some cells displayed decreases in overall GCaMP3 fluorescence and several displayed small Ca^{2+} oscillations. Nonetheless, sustained increases in Ca^{2+} in cell bodies of *pde6c*^{w59} cones undergoing morphological changes of cell death were not detected during our *in vivo* time-lapse experiments nor were elevated perikaryal $[Ca^{2+}]_i$ levels observed in *Pde6β*^{rd1} mouse rods. This finding is in stark contrast to the pronounced $[Ca^{2+}]_i$ increases elicited in non-mutant cones by excessive laser exposure (Figure 2). Hence, our observations argue against a major role of depolarization, voltage-activated Ca^{2+} influx, mitochondrial overload and Ca^{2+} release from internal stores in cone and rod death driven by Pde6 mutations. Consistent with this, elimination of Ca^{2+} influx through L-type channels slightly delayed, but did not prevent, *rd1* degeneration.[24]

We observed dramatic transient increases in $[Ca^{2+}]_i$ in WT and in pre-degeneration *pde6c*^{w59} cones. This finding indicates that Ca^{2+} homeostasis in photoreceptors is dynamically regulated and similar in light-adapted and unstimulated photoreceptors. Thus, the Ca^{2+} changes that we report appear independent of phototransduction. Although future studies will explore possible sources for such Ca^{2+} flashes, potential sources include voltage-gated Ca^{2+} channels, receptor-mediated and/or store-operated Ca^{2+} influx from the extracellular space channels, as well as Ca^{2+} release from internal stores gated by ryanodine/inositol triphosphate release Ca^{2+} channels.[22] Numerous studies focusing on non-excitable and excitable cells[25] suggest that internal compartments represent major contributors to spontaneous elevations in $[Ca^{2+}]_i$. 'Sparks' or 'puffs' have been proposed to regulate cardiac and skeletal muscle excitation–contraction coupling, vascular tone regulation, membrane excitability and neuronal secretion, but were also implicated in regulation of developmental changes, plasticity or cell to cell communication.[25] Ryanodine-sensitive Ca^{2+} stores are present in photoreceptors and have been proposed to help maintain Ca^{2+} levels within a physiological range optimal for normal function under dim lights,[26] whereas store-operated calcium entry and transient receptor potential channels might have a more significant function under bright and prolonged illumination.[22,27]

In conclusion, we here document new features of Ca^{2+} signaling in cone photoreceptors and address the long-standing question whether Pde6 mutations trigger photoreceptor degeneration through Ca^{2+} -dependent activation of proapoptotic pathways driven by cGMP-induced Ca^{2+} overloads within the cell body. We found that, surprisingly, Pde6 loss does not result in sustained increases in $[Ca^{2+}]_i$ in either mouse rods or zebrafish cones. Our data show that *in vivo* analysis of photoreceptor physiology represents a powerful new tool to study function in normal and diseased retinal tissue.

Materials and Methods

Zebrafish maintenance and mutant isolation. Adult fish and larvae were maintained at 28.5 °C in reverse-osmosis distilled water reconstituted for fish compatibility by addition of salts and vitamins[28] on a 10/14 h dark/light cycle. Unless otherwise noted, all zebrafish strains are homozygous for the *roy orbison* (*roy*) mutation.[29] Fish used in live imaging experiments were maintained in embryo media[28] containing 0.003% 1-phenyl 2-thiourea (PTU) starting at 8–24 h post fertilization (h.p.f.). The *pde6c*^{w59} mutant was originally isolated in a screen of mutagenized-zebrafish using the optokinetic response behavioral assay as described previously.[13] The *pde6c*^{w59} mutation is maintained as heterozygotes and intercrossed to generate homozygous mutants.

Construction of transgenic zebrafish. To express GCaMP3 specifically in cones, we used the Gateway-based Tol2kit[30] and inserted GCaMP3 downstream of the 3.2 Kb of the *TαCP*.[14] The resulting construct was injected into WT zebrafish embryos at the 1–2-cell stage together with Tol2 transposase mRNA.[31] Mosaics were identified at 4 d.p.f. and raised to adulthood. Germline carriers were identified in the F1 generation. To visualize cone morphology, we generated a transgenic line *Tg(Trβ2:tdTomato)* expressing tdTomato in the long-wavelength cones (this paper and Suzuki *et al*., in preparation). The *Trβ2* promoter isolation, clone construction, and the general expression were described previously.[19] Germline carriers were identified from mosaic fish injected with this construct. Both *Tg(TαCP:GCaMP3)* and *Tg(Trβ2:tdTomato)* were crossed into the *pde6c*^{w59} mutant lines. The transgenic line *Tg(TαCP:membrane CFP)* was described previously.[12]

Pde6c^{w59} genotyping. After imaging, zebrafish larval genotypes were verified by PCR analysis followed by restriction enzyme digest, as previously described.[28] Primers were used to create a restriction site for BsaXI in only the mutant locus (forward: 5′-TTGGCCTCTGGAATACTGGCT-3′; reverse: 5′-GTTTGACCAGAACCCGGAAG-3′). PCR products were digested with BsaX1 and genotyped according to its restriction profile.

ERG recordings. ERGs were recorded as described previously.[32] Briefly, 5 and 6 d.p.f. larvae were anesthetized in 0.02% tricaine, and eyes were removed using a fine tungsten wire loop. Excised eyes were then placed in an oxygenated Ringer's solution (in mM; 130 NaCl, 2.5 KCl, 20 $NaHCO_3$, 0.7 $CaCl_2$, 1.0 $MgCl_2$, and 20 glucose), and a glass electrode was positioned directly onto the cornea. After 3 min ($_{min}$) of dark adaptation, eyes were exposed to white light flashes, and their electrical responses were recorded. Data were acquired and processed as described previously.[33] Peak values are listed as the mean ± S.D. from three animals.

Live time-lapse imaging in zebrafish. For time-lapse imaging, transparent PTU-treated 5–6 d.p.f. larvae were embedded in a drop of 1% low melting point agarose in embryo media. After solidifying, the agarose was covered

with embryo media containing 0.003% PTU and 0.02% (w/v) tricaine. Live time-lapse imaging experiments were performed on an Olympus FV1000MPE multiphoton laser scanning microscope equipped with a $\times 25$ (NA 1.0) long working distance water objective. Images of the *Tg(Trβ2:tdTomato; TαCP: GCaMP3)* double transgenics were acquired using a red/green filter cube at 890 nm wavelength. For the extended time-lapse experiments, images stacks of 30–40 μm (1 μm per slice) were taken every 20 min for 9 h. Single image slices were taken for the shorter time-lapse experiments, which require rapid sampling every 5 s for 15–30 min.

Image processing and analysis. Image processing and analysis was carried out using the ImageJ (Fiji; http://fiji.sc/Fiji) software.[34] Dying *pde6c*^{w59} cells were identified by examining images collected from the extended 9-hour time-lapse experiments. Images were Z-projected using 7–10 stacks at 1 μm depth, for a total of 7–10 μm depth depending on the shape of the cell. The Z-projected images were adjusted to correct for xy drift using the 'stack reg' function, and further corrected for bleaching using the EMBL tools 'bleach correction' function with the tdTomato image selected as a reference (using the 'simple ratio' setting with background set to 0.0). These adjustments were done using the entire image prior to cropping to focus on the dying cell(s). Regions of interest (ROIs) were placed on the cell body of the dying cell and the mean intensity (gray value) measurements were taken. Due to the shape changes these cells undergo, we used the center of the cell body to ensure that the cell continued to be inside the ROI throughout the dying process. Percent change in fluorescence is calculated as $((F_x–F_0)/F_0 \times 100\%)$ where F_x is the mean florescence intensity at time point x and F_0 is the starting fluorescence at time = 0.

For generating kymographs, retina time stacks were first straightened out using the 'Straighten' function in Fiji (Edit > Selection > Straighten) on a segmented line that followed the retina curvature. The synapse and the cell body layers were then separately selected, resliced (Image > Stack > Reslice), and Z-projected (Sum slices) to generate two separate kymographs for each time-lapse. These two kymographs were then combined in two different channels (represented in magenta and green in Figure 5c) and analyzed for flashes. Individual flashing cells, represented as striped columns in the kymographs, were analyzed using the 'Plot Profile' function in Fiji (Analyze > Plot Profile) with options set to vertical profile. Adobe Photoshop CS5 (San Jose, CA, USA) was used to process the images further. Final figures were assembled using Adobe Illustrator CS5.

Ca^{2+} measurements in mouse rods. $[Ca^{2+}]_i$ in acutely isolated mouse rods was measured as described previously.[22] Briefly, postnatal day P8–P10 and P14–P21, *C57Bl6J* (*C57*) and *Pde6β*^{rd1} (*rd1*) mice (Jackson Laboratories, Bar Harbor, ME, USA) were killed, enucleated and the retinas were treated with papain (30–50 U/ml; Worthington, Freehold, NJ, USA; 1 h at room temperature). Acutely isolated photoreceptor cells with intact somas were identified based on their size and morphology (Figure 3b;[22]).The number of mice (*N*) and cells (*n*) in each group was: C57 (P8–10): $N = 3$, $n = 122$; *rd1* (P8–10): $N = 7$, $n = 186$; C57 (P14–21): $N = 3$, $n = 126$; *rd1* (P14–21): $N = 3$, $n = 27$. Following trituration, cells were plated on concanavalin A-coated (0.2 mg/ml; Sigma, St. Louis, MO, USA) coverslips, loaded with fura-2 AM (1–5 μM; Invitrogen, Life Technologies, Grand Island, NY, USA) for 30 min, and washed for 30 min in dye-free L-15 medium at room temperature. Fluorescence was measured using 340 and 380 nm excitation filters (Chroma, Brattleboro, VT, USA), whereas emission was high-pass filtered at 510 nm and captured with cooled digital CCD cameras (HQ2, Photometrics, Tucson, AZ, USA). Data acquisition (10 pairs of images/min) and fluorescence ratio calculations with background subtraction in ROIs encompassing the rod perikaryon were performed with NIS Elements (Melville, NY, USA). Calibration of cytosolic free $[Ca^{2+}]_i$ was carried out by using 10 μM ionomycin in combination with 0 Ca^{2+}/1 mM EGTA followed by 10 mM Ca^{2+} (Figure 3a;[35]). The apparent free $[Ca^{2+}]_i$ was determined from the equation $[Ca^{2+}]_i = ((R—R_{min})/(R_{max}—R)) \times \beta \times Kd$, where *R* is the ratio of emission intensity at 510 nm evoked by 340 nm excitation *versus* emission intensity at 510 nm evoked by 380 nm excitation; R_{min} is the ratio at zero free Ca^{2+}; R_{max} is the ratio at saturating Ca^{2+}; *Kd* the dissociation constant for Ca^{2+} binding to fura-2 in the presence of millimolar Mg^{2+} was taken from the literature (224 nM;[35,36]); $\beta = (F380_{max}/F380_{min})$. R, R_{min}, R_{max}, and β were measured and calculated for each ROI (cell) separately. Baseline values were established for each cell by averaging baseline $[Ca^{2+}]_i$ over a 5 min period. Group baseline values are averages of individual cell data ± S.E.M.

Conflict of Interest

The authors declare no conflict of interest.

Acknowledgements. Research reported in this manuscript was supported by NEI of the National Institutes of Health under award numbers R01 EY018814 (SEB), Core Grant P30EY001730 (UW), RO1 EY14358 (SS), R01 EY13870 (DEK), EY022076 (DEK), Core Grant EY014800 (Moran Eye Center) and also Knights Templar Foundation and International Retina Research Foundation (PB). The content is solely the responsibility of the authors and does not necessarily represent the official views of the National Institutes of Health. We thank Ashley George, and Drs. Gordon Fain, Jim Hurley and Whitney Cleghorn for suggestions on the manuscript.

Author Contributions

EM, AL, and GS conducted zebrafish experiments. PB made calcium measurements from mouse rods. SS generated the *Trβ2:tdTomato* transgenic zebrafish. SEB conceived and directed research. EM, AL, PB, DK and SEB analyzed data. Paper was written by SEB with major contributions from EM, DK, AL, and PB.

1. Keeler CE. The inheritance of a retinal abnormality in white mice. *Proc Natl Acad Sci USA* 1924; **10**: 329–333.
2. Pittler SJ, Keeler CE, Sidman RL, Baehr W. PCR analysis of DNA from 70-year-old sections of rodless retina demonstrates identity with the mouse rd defect. *Proc Natl Acad Sci USA* 1993; **90**: 9616–9619.
3. Bowes C, Li T, Danciger M, Baxter LC, Applebury ML, Farber DB. Retinal degeneration in the rd mouse is caused by a defect in the beta subunit of rod cGMP-phosphodiesterase. *Nature* 1990; **347**: 677–680.
4. Pittler SJ, Baehr W. Identification of a nonsense mutation in the rod photoreceptor cGMP phosphodiesterase beta-subunit gene of the rd mouse. *Proc Natl Acad Sci USA* 1991; **88**: 8322–8326.
5. Trifunovic D, Dengler K, Michalakis S, Zrenner E, Wissinger B, Paquet-Durand F. cGMP-dependent cone photoreceptor degeneration in the cpfl1 mouse retina. *J Comp Neurol* 2010; **518**: 3604–3617.
6. Davis RJ, Tosi J, Janisch KM, Kasanuki JM, Wang NK, Kong J *et al.* Functional rescue of degenerating photoreceptors in mice homozygous for a hypomorphic cGMP phosphodiesterase 6 b allele (Pde6bH620Q). *Invest Ophthalmol Vis Sci* 2008; **49**: 5067–5076.
7. Paquet-Durand F, Beck S, Michalakis S, Goldmann T, Huber G, Muhlfriedel R *et al.* A key role for cyclic nucleotide gated (CNG) channels in cGMP-related retinitis pigmentosa. *Hum Mol Genet* 2011; **20**: 941–947.
8. Paquet-Durand F, Silva J, Talukdar T, Johnson LE, Azadi S, van Veen T *et al.* Excessive activation of poly(ADP-ribose) polymerase contributes to inherited photoreceptor degeneration in the retinal degeneration 1 mouse. *J Neurosci* 2007; **27**: 10311–10319.
9. Paquet-Durand F, Azadi S, Hauck SM, Ueffing M, van Veen T, Ekstrom P. Calpain is activated in degenerating photoreceptors in the rd1 mouse. *J Neurochem* 2006; **96**: 802–814.
10. Barabas P, Cutler Peck C, Krizaj D. Do calcium channel blockers rescue dying photoreceptors in the Pde6b (rd1) mouse? *Adv Exp Med Biol* 2010; **664**: 491–499.
11. Doonan F, Donovan M, Cotter TG. Activation of multiple pathways during photoreceptor apoptosis in the rd mouse. *Invest Ophthalmol Vis Sci* 2005; **46**: 3530–3538.
12. Lewis A, Williams P, Lawrence O, Wong RO, Brockerhoff SE. Wild-type cone photoreceptors persist despite neighboring mutant cone degeneration. *J Neurosci* 2010; **30**: 382–389.
13. Stearns G, Evangelista M, Fadool JM, Brockerhoff SE. A mutation in the cone-specific pde6 gene causes rapid cone photoreceptor degeneration in zebrafish. *J Neurosci* 2007; **27**: 13866–13874.
14. Kennedy BN, Alvarez Y, Brockerhoff SE, Stearns GW, Sapetto-Rebow B, Taylor MR *et al.* Identification of a zebrafish cone photoreceptor-specific promoter and genetic rescue of achromatopsia in the nof mutant. *Invest Ophthalmol Vis Sci* 2007; **48**: 522–529.
15. Tian L, Hires SA, Mao T, Huber D, Chiappe ME, Chalasani SH *et al.* Imaging neural activity in worms, flies and mice with improved GCaMP calcium indicators. *Nat Methods* 2009; **6**: 875–881.
16. Borghuis BG, Tian L, Xu Y, Nikonov SS, Vardi N, Zemelman BV *et al.* Imaging light responses of targeted neuron populations in the rodent retina. *J Neurosci* 2011; **31**: 2855–2867.
17. Esterberg R, Hailey DW, Coffin AB, Raible DW, Rubel EW. Disruption of intracellular calcium regulation is integral to aminoglycoside-induced hair cell death. *J Neurosci* 2013; **33**: 7513–7525.
18. Weitz AC, Behrend MR, Lee NS, Klein RL, Chiodo VA, Hauswirth WW *et al.* Imaging the response of the retina to electrical stimulation with genetically encoded calcium indicators. *J Neurophysiol* 2013; **109**: 1979–1988.

19. Williams PR, Suzuki SC, Yoshimatsu T, Lawrence OT, Waldron SJ, Parsons MJ *et al. In vivo* development of outer retinal synapses in the absence of glial contact. *J Neurosci* 2010; **30**: 11951–11961.
20. Lewis A, Wilson N, Stearns G, Johnson N, Nelson R, Brockerhoff SE. Celsr3 is required for normal development of GABA circuits in the inner retina. *PLoS Genet* 2011; **7**: e1002239.
21. Sahaboglu A, Paquet-Durand O, Dietter J, Dengler K, Bernhard-Kurz S, Ekstrom PA *et al.* Retinitis pigmentosa: rapid neurodegeneration is governed by slow cell death mechanisms. *Cell Death Dis* 2013; **4**: e488.
22. Molnar T, Barabas P, Birnbaumer L, Punzo C, Kefalov V, Krizaj D. Store-operated channels regulate intracellular calcium in mammalian rods. *J Physiol* 2012; **590**(Pt 15): 3465–3481.
23. Rizzuto R, De Stefani D, Raffaello A, Mammucari C. Mitochondria as sensors and regulators of calcium signalling. *Nat Rev Mol Cell Biol* 2012; **13**: 566–578.
24. Read DS, McCall MA, Gregg RG. Absence of voltage-dependent calcium channels delays photoreceptor degeneration in rd mice. *Exp Eye Res* 2002; **75**: 415–420.
25. Ross WN. Understanding calcium waves and sparks in central neurons. *Nat Rev Neurosci* 2012; **13**: 157–168.
26. Krizaj D, Lai FA, Copenhagen DR. Ryanodine stores and calcium regulation in the inner segments of salamander rods and cones. *J Physiol* 2003; **547**(Pt 3): 761–774.
27. Krizaj D. Calcium stores in vertebrate photoreceptors. *Adv Exp Med Biol* 2012; **740**: 873–889.
28. Westerfield M. *The Zebrafish Book: A Guide for the Laboratory Use of Zebrafish (Brachydanio rerio).* University of Oregon Press: Eugene, Orgeon, USA, 1995.
29. Ren JQ, McCarthy WR, Zhang H, Adolph AR, Li L. Behavioral visual responses of wild-type and hypopigmented zebrafish. *Vision Res* 2002; **42**: 293–299.
30. Kwan KM, Fujimoto E, Grabher C, Mangum BD, Hardy ME, Campbell DS *et al.* The Tol2kit: a multisite gateway-based construction kit for Tol2 transposon transgenesis constructs. *Dev Dyn* 2007; **236**: 3088–3099.
31. Kawakami K, Shima A, Kawakami N. Identification of a functional transposase of the Tol2 element, an Ac-like element from the Japanese medaka fish, and its transposition in the zebrafish germ lineage. *Proc Natl Acad Sci USA* 2000; **97**: 11403–11408.
32. Wong KY, Gray J, Hayward CJ, Adolph AR, Dowling JE. Glutamatergic mechanisms in the outer retina of larval zebrafish: analysis of electroretinogram b- and d-waves using a novel preparation. *Zebrafish* 2004; **1**: 121–131.
33. Van Epps HA, Yim CM, Hurley JB, Brockerhoff SE. Investigations of photoreceptor synaptic transmission and light adaptation in the zebrafish visual mutant nrc. *Invest Ophthalmol Vis Sci* 2001; **42**: 868–874.
34. Schindelin J, Arganda-Carreras I, Frise E, Kaynig V, Longair M, Pietzsch T *et al.* Fiji: an open-source platform for biological-image analysis. *Nat Methods* 2012; **9**: 676–682.
35. Grynkiewicz G, Poenie M, Tsien RY. A new generation of Ca2+ indicators with greatly improved fluorescence properties. *J Biol Chem* 1985; **260**: 3440–3450.
36. Neher E. The use of fura-2 for estimating Ca buffers and Ca fluxes. *Neuropharmacology* 1995; **34**: 1423–1442.

Supplementary Information accompanies this paper on Cell Death and Disease website (http://www.nature.com/cddis)